Dynamic imaging of lateral diffusion by electron spin resonance and study of rotational dynamics in model membranes

Effect of cholesterol

Y.-K. Shin and Jack H. Freed
Baker Laboratory of Chemistry, Cornell University, Ithaca, New York 14853

ABSTRACT The effects of cholesterol on the dynamics and the structural properties of two different spin probes, the sterol type CSL and the phospholipid type 16-PC, in POPC/cholesterol oriented multilayer model membranes were examined. Our results are consistent with a nonideal solution containing cholesterol-rich clusters created by the self association of cholesterol in POPC model membranes. The lateral diffusion coefficient D of the spin probes was measured over the temperature range of 15 to 60°C and over the concentration range of 0 to 30 mol % of cholesterol in the model membrane by the electron spin resonance (ESR) imaging method. The rotational diffusion coefficients (including $R_\perp$) and the order parameter S were determined utilizing a nonlinear least square ESR spectral simulation method. D, $R_\perp$ and S of CSL deviate considerably from linear dependence on mole percent cholesterol. The D of CSL was decreased by a factor of four at 15°C and a factor of two at 60°C for concentrations of cholesterol over 10 mol %, whereas those of 16-PC were hardly affected. Cholesterol decreased $R_\perp$ by a factor of 10 at 30 mol % of cholesterol, but it increased slightly that of 16-PC. A significant increase of S for CSL due to the presence of cholesterol was observed. It is shown how the difference in variation of S for CSL vs. 16-PC with composition may be interpreted in terms of their respective activity coefficients, and how a single universal linear relation is obtained for the S of both probes in terms of a scaled temperature. Simple but general correlations of D and of $R_\perp$ with S were also found, which aid in the interpretation of these diffusion coefficients.

INTRODUCTION

The physical properties of phosphatidylcholine model membranes containing cholesterol have been the subject of extensive studies involving a range of techniques. The techniques that have been used to study the phase behavior are calorimetry (1, 2), spin-labeling electron spin resonance (ESR) (3–6), fluorescence (7), freeze fracture electron microscopy (7, 8), x-ray and electron diffraction (9), and recently, Raman spectroscopy (10), as well as neutron scattering along with freeze fracture electron microscopy (11).

A conspicuous phase boundary in the temperature-composition phase diagram was found at ~20 mol % of cholesterol in phosphatidylcholine model membranes below the main chain melting temperature (T_m) (2–9), although it had earlier been believed that there was a phase boundary around 30 mol % (12). This phase boundary has similar characteristics to the main chain melting phase transition: that is, it is a kind of gel-to-liquid crystalline phase boundary, implying that it is a considerably disordered fluid state above 20 mol % of cholesterol. On the other hand, it is a gel phase below 20 mol %. There are two solid phases (tilted $L_{\beta'}$ and nontilted L_β phases) which coexist in the region where cholesterol is <20 mol % and at temperatures below the pretransition temperature (T_p) (7, 11), whereas a cholesterol-rich liquid crystaline phase ($P_{\beta'}$) and a pure phospholipid gel phase ($L_{\beta'}$) coexist at temperatures between T_m and T_p (with $T_p \sim T_m - 10°C$) (4, 5, 8). But the x-ray and electron diffraction studies did not confirm the coexistence of two phases in this region (9). Based on spectroscopic evidence, the acyl chain tilt begins to disappear with the presence of ~5–8 mol % of cholesterol (9, 11).

The phase behavior of model membranes containing cholesterol in the L_α liquid crystalline state (above T_m) has not been clearly established as yet. It was pointed out previously (11) that this might partly be because of the experimental difficulty of detecting fluid–fluid immiscibility by the commonly used spectroscopic methods. There have been a few reports suggesting fluid–fluid phase separation (5, 7, 13). A homogeneous single phase also has been suggested experimentally (9, 11).

In addition to the phase behavior, the dynamical properties and ordering of the molecules in the bilayer have their own physical importance. The rotational dynamics and ordering properties of lipid molecules or cholesterol analogues in the binary mixture have been investigated mainly by magnetic resonance (14, 15) and fluorescence techniques (16, 17). It had been shown that cholesterol decreased the fluidity of the fatty acyl chain in the liquid crystalline state. It has been possible to separate several aspects of the rotational dynamics rather than to use the general term fluidity. In the fluorescence study the rotational motion was analyzed by a model of wobbling motion confined within a cone (16). In this model the

0006-3495/89/03/537/14 $2.00

viscosity within the cone remained constant, but the cone angle decreased with addition of cholesterol. The anisotropic rotational diffusion model defines parallel and perpendicular rotational diffusion coefficients, as well as the ordering potential. The ESR study based on spectral simulation, utilized the model of anisotropic rotational diffusion in an orienting potential. It revealed increased ordering, but only a small effect of cholesterol on the rotational motion (15). Various studies have agreed that the major effect of cholesterol is to reduce the angular range for rotational motion without decreasing mobility substantially (14, 15, 16). On the other hand, in the gel phase cholesterol induces local disorder and enhances the rotational motion. Generally, fully hydrated bilayers have been used so far. But the careful study of low water content DPPC samples by ESR showed effects of cholesterol on rotational dynamics similar to that in the liquid crystalline phase even in the gel phase (15).

Another important dynamical property of the bilayer containing cholesterol is the lateral diffusion of the constituent molecules. The effect of cholesterol on the diffusion of the phospholipid molecules has drawn much attention because it is directly related to understanding the transport properties in biological membranes. It has been studied by fluorescence recovery after photobleaching (FRAP) (18–21), pulsed-NMR spin echoes (PNSE) (22, 23), and fluorescence correlation spectroscopy (24). Below T_m one or two orders of magnitude increase of the lateral diffusion coefficients of the phospholipid analogue above 20 mol % of cholesterol has been found, supporting the idea that it is a fluid phase even below T_m. Also, cholesterol decreased the lateral diffusion coefficient about factors of two at 20 mol % or greater, above T_m (19, 24). In another study, a sterol type fluorescence probe was found to behave in exactly the same way as a phospholipid type probe (20, 21). However PNSE gave significantly different results for the self diffusion of phospholipid; the addition of cholesterol was observed to increase the diffusion rates of DPPC up to 10 mol % above T_m, and then to decrease it above 10 mol % (22). For the unsaturated acyl chain phosphatidylcholines (POPC, DOPC) the lateral diffusion was observed only to increase slightly with cholesterol concentration in the liquid crystalline state (23).

We have developed an ESR-imaging method for measuring the translational diffusion coefficients of ordered systems such as liquid crystals and lipids (25, 26). We have demonstrated that our method is one of the useful spectroscopic techniques for studying lateral diffusion of model membranes (26). We pointed out in our previous work (26) that one could also simultaneously obtain the rotational diffusion coefficients and the order parameters in the usual fashion (e.g., 15, 27) by analyzing the magnetic field gradient-off spectra which are just the normal ESR spectra. Such a combined study can be expected to provide better insight into the dynamic properties of membranes. In this work we present an application of the ESR imaging method for lateral diffusion along with an improved spectral simulation method for ordering and rotational diffusion based upon nonlinear least square fitting (28), to oriented model membranes of POPC containing cholesterol.

The POPC molecule has one saturated acyl chain and one unsaturated chain, as is characteristic of naturally abundant phosphatidylcholines in biological membranes. Here we concentrate on the liquid crystalline state for two reasons: (*a*) Most real biological membranes exist in this state (7), so an understanding of the dynamical properties of both cholesterol and phospholipid in an unsaturated phospholipid model membrane such as POPC in this phase would be directly relevant to the role of cholesterol in biological membranes (7). (*b*) Our ESR imaging method is well suited to measure diffusion coefficients in the liquid crystalline state of the membranes which range from 10^{-9} cm^2 s^{-1} to 10^{-7} cm^2 s^{-1}.

We used two types of spin probes, CSL and 16-PC (Fig. 1). CSL is a good spin probe to reveal the dynamical features of cholesterol in model membranes (6, 15). The other probe is 16-PC, which is frequently used to study the properties of phosphatidylcholine model membranes by ESR (27, 29). From a comparison of the behavior of these two spin probes we could hope to better understand the properties of model membranes containing cholesterol in the liquid crystalline state.

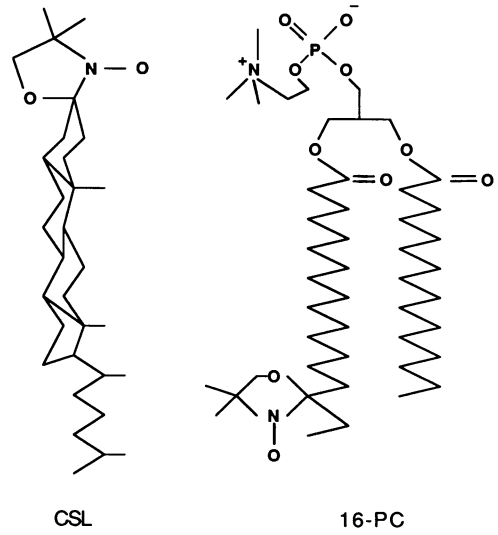

FIGURE 1 Structure of cholestane (CSL) and 16-PC spin probes.

EXPERIMENTAL METHODS

Materials

1-Palmitoyl-2-oleoyl-*sn*-glycero-phosphatidylcholine (POPC) was purchased from Avanti Polar Lipid Inc., Birmingham, AL, and was used without further purification. Cholesterol was obtained from Calbiochem-Behring Corp., La Jolla, CA, and recrystallized in ethanol. The 3-doxyl derivative of cholestan-3-one (CSL) was purchased from Syva Co., Palo Alto, CA, and 1-palmitoyl-2-(16-doxyl stearoyl)phosphatidylcholine (16-PC) was a gift from Professor G. W. Feigenson, Department of Biochemistry, Cornell University, who synthesized it according to standard methods (30). The purity of the 16-PC was tested by thin layer chromatography, and it was found to contain <2% impurity.

Sample preparation

The two basic sample requirements in our ESR imaging experiment are (*a*) the spin probe distribution is localized at the middle of the sample, (*b*) the sample is a well-aligned homeotropic monodomain of lipid multilayers. Because the experimental time (Δt) required is proportional to the square of the initial width of the spin probe distribution (δ^2) (26), the initial width has to be as thin as possible to minimize Δt. To prepare samples satisfying such requirements, we followed the modified evaporation-compression technique explained in our previous work (26). It is based on the hydration-evaporation technique (31) and the compression alignment technique of Tanaka and Freed (27). For details of the procedures and characterization methods see references 26 and 27. The spin probe concentration of the CSL was 0.75 mol % and that of the 16-PC was 0.50 mol %. The ESR spectra of both samples did not show any lineshape broadening due to Heisenberg spin exchange at those concentrations. The water content of the sample was determined by weighing after the ESR measurement (26). The POPC/cholesterol samples were found to have 15–20% water by weight.

Instrumental and data collection

A Varian Associates, Inc. (Palo Alto, CA) E-12 spectrometer was used for the experiments. The spectra were taken in the first derivative mode with 100 kHz field modulation, with a microwave power of ~5 mW, and with a modulation amplitude ~0.8 G. Homemade figure-eight gradient coils, which produced a linear field gradient of 36 G/cm at 2.0 A current, were used (25, 26). A standard Bruker Instruments, Inc. (Billerica, MA) nitrogen flowing temperature control unit was used to regulate the sample temperature. The temperature control and variation was achieved by using an 11-mm OD single wall quartz dewar and by monitoring the temperature with a thermocouple inserted inside the dewar from the bottom. The temperature was controlled to ±0.5°C accuracy. The temperature of the sample was raised ~10°C between successive temperature runs. Data were collected on a model D PC (Leading Edge Inc., Canton, MA) interfaced to an HP3457 multimeter (Hewlett-Packard Co., Loveland, CO). All spectra were digitized to 1,024 points, had 100-G sweep widths, and 60-s sweep times. Two gradient-on spectra were recorded consecutively and one gradient-off reference spectrum was taken subsequently. About 20 gradient-on spectra were recorded at a fixed temperature, and this took ~1 h. Each sample was used for five different temperatures ranging from 15 to 60°C.

Data analysis

Lateral diffusion by ESR imaging. The measurement of diffusion coefficients by ESR imaging is an application that we refer to as "dynamic imaging" (26). It involves two stages. A sample is prepared with an inhomogeneous distribution of spin probes along a given direction. The ESR imaging method is first utilized to obtain the (one-dimensional) concentration profiles at several different times. The imaging method is based on the use of a magnetic field gradient, such that at each spatial point there is a different local resonant frequency. Typical ESR spectra from imaging concentration profiles are shown in references 25 and 26; also shown are the concentration profiles. With the passage of time, this inhomogenous distribution will tend to a homogeneous distribution via translational diffusion. The second stage is to fit the time-dependent concentration profiles to the diffusion equation to obtain the diffusion coefficient. We have shown (26) that the analysis is greatly improved by studying the spatial Fourier Transform of the concentration profiles.

The one-dimensional diffusion equation in Fourier transform or k-space is given by

$$ln|C(k, t_1)| - ln|C(k, t_0)| = -4\pi^2 D k^2 \Delta t, \qquad (1)$$

where $\Delta t = t_1 - t_0$ is the time difference between two measurements and D is the lateral diffusion coefficient in units of cm^2s^{-1}. To obtain the concentration profile $C(k, t_i)$ at a given time in k-space we deconvolute the gradient-on spectrum with the gradient-off spectrum utilizing the convolution theorem in Fourier space:

$$C(k, t_i) = \frac{I_g(k, t_i)}{I_0(k)}, \qquad (2)$$

where $I_g(k)$ is the Fourier transformed gradient-on spectrum and $I_o(k)$ is a Fourier transformed gradient-off spectrum. The lateral diffusion coefficient D is determined by the method described in our previous paper (26). In summary, because we used samples that are well approximated by a Gaussian initial spin probe distribution,

$$C(x) = \frac{C_o}{(2\pi)^{1/2}\delta} \exp\left(-\frac{x^2}{2\delta^2}\right). \qquad (3)$$

The log of the concentration profile in k-space may be written as

$$ln|C(k, t_i)| = \alpha(t_i)\, k^2, \qquad (4)$$

where $\alpha(t_i) = -2\pi^2\delta^2 - 4\pi^2 D\, t_i$. Thus, by plotting $|C(k, t_i)|$ with respect to k^2 one obtains the slope $\alpha(t_i)$. The $\alpha(t_i)$s are related to each other by the diffusion equation (Eq. 1):

$$\alpha(t_i) - \alpha(t_j) = -4\pi^2 D(t_i - t_j). \qquad (5)$$

Thus a plot $\alpha(t_i)$s with respect to t_i yields D. We could estimate the half width at half maximum (HWHM) Γ of the Gaussian concentration distribution by the relation

$$\Gamma(t_i) = \frac{1}{\pi}\sqrt{-\alpha(t_i)\, ln\, 2}, \qquad (6)$$

at a given time t_i. The HWHM's of the Gaussian profiles were about 0.5 mm at the beginning of the measurement. Several examples, illustrating how the $C(k, t_i)$ are analyzed to obtain D, are given in reference 26.

Nonlinear least square spectral simulation. During the course of each experiment we collected the gradient-off spectra. They were analyzed to obtain information on ordering and rotational dynamics utilizing ESR spectral simulation methods (32–34). The ESR simulations were performed utilizing nonlinear least square fitting to obtain the optimum parameters (28). For the spin probes we were using, we followed the axis system conventions described elsewhere (27, 35).

The potential $V(\Omega)$ determining the orientational distribution of the spin probe molecules around the ordering axis in the uniaxially ordered

lipid multilayers can be expanded in a series of Wigner rotation matrix elements, e.g.,

$$-V(\Omega)/kT = \lambda D^2_{00}(\Omega) + \rho(D^2_{02}(\Omega) + D^2_{0-2}(\Omega)) + \ldots, \quad (7)$$

where k is the Boltzmann constant and Ω is an Euler angle specifying the relative orientation between the rotational diffusion axis (it is assumed to coincide with molecular long axis) and ordering axis. The values of the magnetic tensor A used were $A_{z'} = 33.8$ G and $A_{x'}(=A_{y'}) = 5.0$ G for CSL, and $A_{z'} = 33.0$ G and $A_{x'}(=A_{y'}) = 4.9$ G for 16-PC. Those of g were $g_{x'} = 2.0089$, $g_{y'} = 2.0058$, and $g_{z'} = 2.0021$ for both spin probes (27). One can specify the angle (Ψ) between the ordering axis and the applied magnetic field (H_0). All spectra of CSL that were simulated had $\Psi = 0°$, whereas those of 16-PC had $\Psi = 90°$. These values of Ψ had been chosen to minimize the spectral linewidths, thereby enhancing resolution in the imaging experiments.

The first step in the nonlinear least square simulation was to choose reasonable starting values of the four parameters, λ, ρ, the perpendicular rotational diffusion coefficient ($R_\perp$), and the parallel rotational diffusion coefficient ($R_\parallel$). They were chosen simply from previous results for the same probes in DPPC multilayers (27). The fitting process was iterated several times by a Marquard-Levenberg algorithm until a minimum in the least squares was achieved. To insure that a global minimum was achieved and to guard against spurious local minima, the algorithm was restarted several times with a range of different seed values. Convergence to the same final set (to within the experimental uncertainty) was always achieved (except in a few cases where no convergence was obtained). The fits were very sensitive to λ and $R_\perp$ while less sensitive to ρ and $R_\parallel$.

Once we obtained the potential parameters (λ, ρ), we calculated the order parameter defined by

$$S \equiv \langle D^2_{00}(\Omega) \rangle = \int D^2_{00}(\Omega) \exp\left(-\frac{V(\Omega)}{kT}\right) d\Omega \cdot \Big/ \int \exp\left(-\frac{V(\Omega)}{kT}\right) d\Omega, \quad (8)$$

where $D^2_{00}(\Omega) = (1/2)(\cos^2\theta - 1)$. The spectral simulations showed that the values of λ are about an order of magnitude bigger than ρ for CSL. Thus, neglecting ρ and higher order terms, we can simplify the potential expansion to

$$-\frac{V(\Omega)}{kT} \sim \lambda D^2_{00}(\Omega), \quad (9)$$

for which the order parameter S can be written as

$$S \sim \int D^2_{00}(\Omega) \exp(\lambda D^2_{00}(\Omega))\, d\Omega \cdot \Big/ \int \exp(\lambda D^2_{00}(\Omega))\, d\Omega. \quad (10)$$

This integral was calculated numerically. An asymptotic expression, valid for large λ, is given in the Appendix.

RESULTS AND ANALYSIS

General observations

Lateral diffusion

Results were obtained for five different compositions of cholesterol in POPC multilayers, 0, 4, 10, 20, and 30 mol % with CSL spin probe. Using 16-PC probe 0, 10, and 20 mol % were used. The temperature was chosen to be at least 10° above the main chain melting temperature T_m of hydrated POPC. The lateral diffusion coefficients D of CSL in the different mixtures are listed in Table 1. Those of 16-PC are shown in Table 2. One notes that for 0 mol % cholesterol, $D_{CSL}/D_{16\text{-}PC} \sim 1.6$ consistent with the somewhat smaller size of CSL. Semilog plots of the temperature variation of D are shown in Fig. 2, *a* and *b*, respectively. The activation energy for lateral diffusion was calculated for each probe in each mixture. It ranges from 6 to 9 kcal/mol depending on the concentration of cholesterol. There is a noticeable increase of activation energy of CSL (~3 kcal/mol) between 4 and 10 mol %. These values are given in Table 1. Fig. 3 shows the variation of D for each probe at different cholesterol concentrations. 10 mol % of cholesterol decreased the D of CSL by factors of four at 15°C, and factors of two at 60°C. The further addition of cholesterol over 10 mol % was not so effective in reducing D of CSL as it was below 10 mol %. On the other hand, the D of 16-PC at different compositions was almost unaffected at high temperatures, although it decreased slightly at 15 and 25°C. Given that the D of CSL or 16-PC would not be much different from that of cholesterol or phospholipid, respectively, the presence of cholesterol appears to influence the cholesterol diffusion more than that of the phospholipid.

Ordering and rotational diffusion

Spectral simulations were performed for spectra of CSL and 16-PC at all concentrations and temperatures we have studied. The best fitting rotational diffusion coefficients and order parameters of CSL are given in Table 1 and those of 16-PC in Table 2. Some of the simulated spectra are compared with the experimental ones in Fig. 4, *a* and *b*. The activation energy for the $R_\perp$ of CSL is given in Table 1 for the different compositions. Factors of two increase of the activation energies at ~10 mol % of cholesterol compared with that at 0 mol % were found. Fig. 5 shows the variation of $R_\perp$ of CSL with cholesterol. We plot the temperature variation of order parameter S of CSL at different composition in Fig. 6 *a*. The order parameter S of both spin probes appears to decrease linearly with temperature, and to increase with increasing mol % cholesterol.

We used $\Psi = 0°$ CSL spectra for ESR simulation. This means that we are observing the spectrum along the principal ordering axis. For this highly ordered probe the molecular long axis is preferentially along this principal ordering axis. Thus, in this configuration, the spectral shape was very sensitive to the value of $R_\perp$, whereas it was fairly insensitive to $R_\parallel$ (as confirmed by our nonlinear least-square analysis). Thus, we put less emphasis on $R_\parallel$ in analyzing the results of the spectral simulations. For

TABLE 1 Data for the CSL spin probe

T	D	S	λ	ρ	$R_\perp$	$R_\parallel$
°C	$10^{-8}cm^2s^{-1}$				10^7s^{-1}	10^8s^{-1}
	0 mol % cholesterol E_{actD} = 6.30 kcal/mol $E_{actR_\perp}$ = 2.50 kcal/mol					
15.7	3.96 ± 0.33	0.532	2.5105	0.4769	1.766	1.137
25.3	5.88 ± 0.30	0.471	2.1644	0.6705	2.236	0.993
35.0	7.82 ± 0.31	0.452	2.0635	0.6853	2.559	1.091
48.7	12.00 ± 0.51	0.418	1.8933	0.6967	3.087	1.435
63.0	19.10 ± 1.00	0.383	1.7259	0.6492	3.555	1.826
	4 mol % cholesterol E_{actD} = 6.45 kcal/mol $E_{actR_\perp}$ = 2.10 kcal/mol					
14.2	2.40 ± 0.66	0.663	3.4791	0.6681	1.029	1.928
24.0	3.32 ± 0.37	0.635	3.2379	0.5352	1.293	1.866
35.0	5.10 ± 0.56	0.599	2.9517	0.6100	1.463	2.035
48.0	8.31 ± 1.31	0.566	2.7264	0.4904	1.824	2.213
60.7	11.70 ± 1.40	0.536	2.5370	0.4384	2.026	2.715
	10 mol % cholesterol E_{actD} = 9.73 kcal/mol $E_{actR_\perp}$ = 5.06 kcal/mol					
14.8	0.96 ± 0.21	0.787	5.1900	0.6117	0.385	1.878
25.1	1.47 ± 0.22	0.753	4.5771	0.3633	0.550	2.430
35.8	2.78 ± 0.33	0.722	4.1254	0.2090	0.728	3.144
48.8	5.55 ± 0.85	0.683	3.6799	0.1461	0.926	4.067
60.9	9.43 ± 1.04	0.651	3.3721	0.0080	1.171	7.795
	20 mol % cholesterol E_{actD} = 9.84 kcal/mol $E_{actR_\perp}$ = 5.73 kcal/mol					
15.0	0.98 ± 0.15	0.825	6.1778	0.9221	0.241	1.368
25.3	1.58 ± 0.17	0.792	5.3010	0.7192	0.349	1.806
35.9	3.21 ± 0.22	0.763	4.7422	0.4073	0.480	2.597
48.8	5.93 ± 0.26	0.725	4.1700	0.1691	0.649	3.853
60.2	9.53 ± 0.43	0.691	3.7693	0.1324	0.816	6.221
	30 mol % cholesterol E_{actD} = 9.94 kcal/mol $E_{actR_\perp}$ = 5.42 kcal/mol					
15.4	0.88 ± 0.17	0.852	7.1719	1.6686	0.156	0.963
25.2	1.38 ± 0.16	0.830	6.3300	0.7500	0.240	1.621
35.0	2.03 ± 0.19	0.812	5.8118	0.3558	0.312	2.320
47.7	4.34 ± 0.27	0.784	5.1360	0.1698	0.413	3.372
60.3	9.17 ± 0.33	0.745	4.4485	0.1809	0.531	3.692

TABLE 2 Data for 16-PC spin probe

T	D	S	λ	ρ	$R_\perp$
°C	$10^{-8}cm^2s^{-1}$				10^8
	0 mol % cholesterol E_{actD} = 6.15 kcal/mol				
15.8	2.45 ± 0.57	0.172	0.7995	0.1956	3.86
26.0	3.53 ± 0.50	0.141	0.6631	0.1734	4.44
36.2	5.09 ± 0.55	0.120	0.6368	−0.5382	4.94
49.5	7.39 ± 1.11	0.074	0.3915	−0.3748	7.66
62.5	11.00 ± 1.60	0.027	0.4529	1.1179	14.11
	10 mol % cholesterol E_{actD} = 7.87 kcal/mol				
15.5	1.61 ± 0.43	0.214	0.9937	−0.2864	4.15
25.6	2.92 ± 0.61	0.191	0.8956	−0.3041	5.04
35.9	4.57 ± 0.82	0.174	1.0168	−0.9411	6.77
48.6	7.25 ± 1.22	0.101	1.1781	−1.7804	14.13
60.8	10.60 ± 1.80	0.084	1.1394	−1.8332	17.14
	20 mol % cholesterol E_{actD} = 8.92 kcal/mol				
15.0	1.20 ± 0.50	0.268	1.2396	−0.3565	4.85
25.6	2.57 ± 0.54	0.241	1.1138	−0.3124	5.97
36.0	4.69 ± 0.87	0.218	1.6264	−1.7173	13.41
48.8	7.29 ± 1.10	0.157	0.9519	−0.9580	21.50
60.8	10.40 ± 1.30	0.150	0.8864	−0.8728	23.70

16-PC, the spectral lineshape was found to be sensitive to $R_\perp$ but almost insensitive to the anisotropy ratio for rotational diffusion, $R_\parallel/R_\perp$ (again from nonlinear least-square analysis). A model of isotropic Brownian rotational reorientation was therefore employed to simulate 16-PC spectra. The activation energy for $R_\perp$ of 16-PC was also found to increase somewhat with increase of mole percent cholesterol but less than the case for CSL. However, over the temperature range studied, $R_\perp$ of 16-PC actually increased slightly with mole percent cholesterol, whereas that for CSL decreased very substantially. The order parameter S, for 16-PC was observed to increase considerably with mole percent cholesterol as was the case for CSL.

Empirical relations and correlations

Order parameter and activity coefficients

One is struck by very nearly parallel straight-line fits of S for CSL vs. temperature (cf. Fig. 6 *a*). That is, the slope

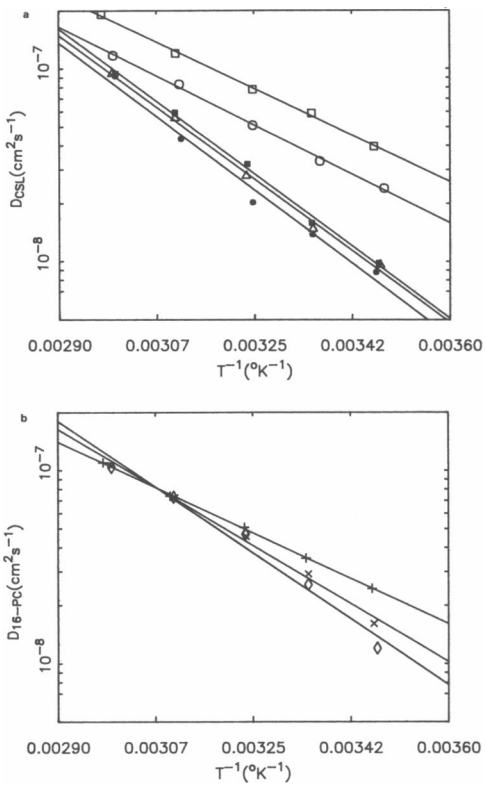

FIGURE 2 (*a*) Semilog plots of D_{CSL} vs. T^{-1}. Cholesterol concentrations in POPC model membrane are 0 (□), 4 (○), 10 (△), 20 (■), and 30 mol % (●). (*b*) Same type of plots as *a* except the spin probe is 16-PC; 0 (+), 10 (×), 20 (◊) mol % of cholesterol in POPC model membranes.

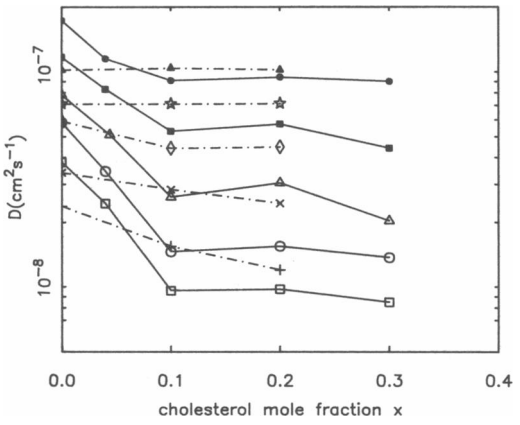

FIGURE 3 Plots of the variation of D_{CSL} and $D_{16\text{-}PC}$ with cholesterol mole fraction x at different temperatures; for CSL, 15 (□), 25 (○), 35 (△), 48 (■), and 60°C (●), and for 16-PC, 15 (+), 25 (×), 35 (◊), 48 (☆), and 60°C (▲). $D_{16\text{-}PC}$ shows little change in the presence of cholesterol. Data used were interpolated by Spline interpolation from those in Tables 1 and 2.

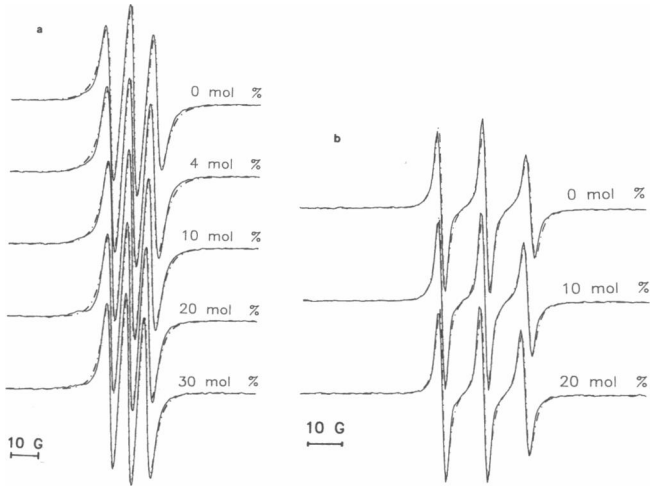

FIGURE 4 (*a*) Comparison of experimental spectra of CSL (—), at 25°C, with simulated ones (—·—) at different concentrations. The angle Ψ is 0°. There is noticeable decrease of hyperfine splitting with increase of cholesterol concentration. (*b*) Comparison of experimental spectra (—) of 16-PC, at 25°C, with simulated ones (—·—).

$(\partial S/\partial T)_x$ does not depend on the composition (except for a small deviation at 30 mol %). Let us arbitrarily define reference temperatures $T_1^*(x)$ and $T_0^*(x)$, which are the extrapolated temperatures corresponding to $S = 1$ and $S = 0$ at a given cholesterol mole fraction, x. Obviously $T_1^*(x)$ and $T_0^*(x)$ are different from composition to composition, but the difference $T_0^*(x) - T_1^*(x)$ must remain constant for all compositions, since the slope $(\partial S/\partial T)_x$ is independent of composition. Thus, we may write the temperature dependence of S in the following

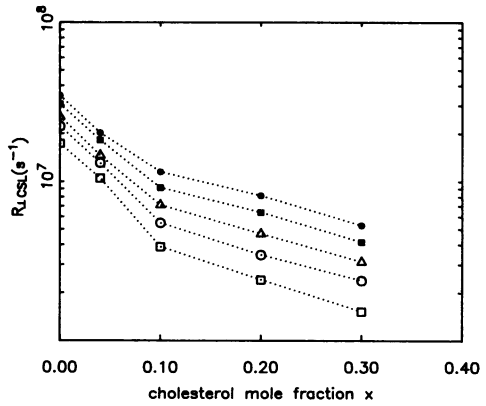

FIGURE 5 Plots of the variation of $R_\perp$ of CSL with cholesterol concentration at different temperatures; 15 (□), 25 (○), 35 (△), 48 (■), and 60°C (●). The behavior of each curve is quite similar to that of D_{CSL} (cf. Fig. 3).

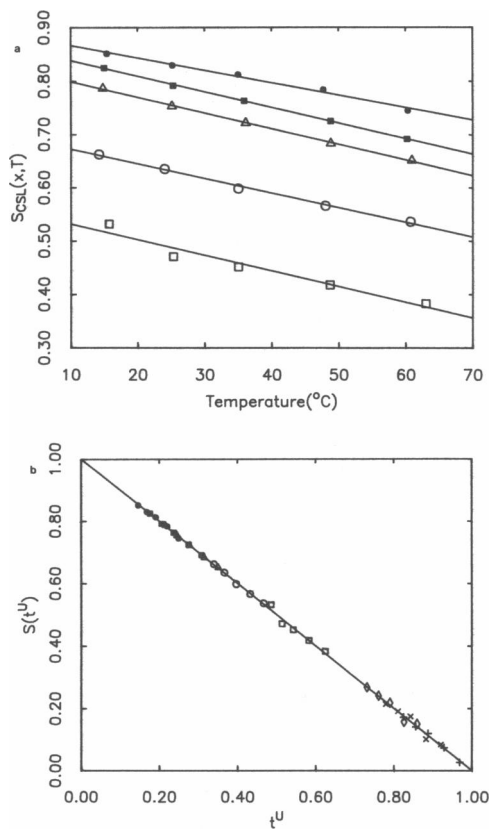

FIGURE 6 (*a*) Plots of temperature dependence of order parameter S of CSL at different compositions; 0 (□), 4 (○), 10 (△), 20 (■), and 30 mol % (●). The slopes are all the same except at 30 mol % where it is slightly smaller than the others. (*b*) Plot of $S(t^U)$ vs. t^U for CSL and 16-PC. Different symbols denote different compositions: for CSL, 0 (□), 4 (○), 10 (△), 20 (■), and 30 mol % (●), and for 16-PC, 0 (+), 10 (×), and 20 (◇) mol %.

form.

$$S(x, T) = 1 - a[T - T_1^*(x)], \text{ for } x \text{ constant}, \quad (11)$$

where $a = 1/[T_0^*(x) - T_1^*(x)] = 2.77 \pm 0.26 \times 10^{-3}$°K. The values of $T_0^*(x)$ and $T_1^*(x)$ are given in Table 3. If we define the scaled temperature $t^U \equiv [T - T_1^*(x)]/[T_0^*(x) - T_1^*(x)]$ (36), then S is simply

$$S(t^U) = 1 - t^U. \quad (12)$$

This scaled equation tells us that the *disorder parameter* $1 - S(t^U)$ is exactly the scaled temperature t^U, and this behavior is universal for nearly all compositions. Thus the ordering effect of cholesterol can be thought of simply as equivalent to a shift of the temperature scale. This universal behavior $S(T)$ vs. t^U is depicted in Fig. 6 *b* for all our data on CSL (as well as 16-PC, see below). (A simple relation between ordering potential λ of CSL and temperature is suggested in the Appendix.)

TABLE 3 Values of $T_1^*(x)$ and $T_2^*(x)$

x (cholesterol)	$T_1^*(x)$	$T_0^*(x)$
	°C	°C
	CSL spin probe	
0.0	−150	191
0.04	−110	255
0.1	−58	281
0.2	−45	296
0.3	−47	385
	16-PC spin probe	
0.0	−252	73
0.1	−235	87
0.2	−246	111

Compare with text and with Eq. 11.

Fig. 7 *a* is a plot of S for CSL vs. cholesterol mole fraction x. The change of order parameter with cholesterol: $S(x, T) - S(0, T)$ is found to vary with x but to be independent of T. The order parameter S increases sharply up to 10 mol %, but S is not very sensitive to further addition of cholesterol. We found that a "Langmuir isotherm" type equation fits the behavior of $S(x, T) - S(0, T)$ vs. x:

$$S(x, T) - S(0, T) = \frac{bx}{1 + cx}, \text{ for } T \text{ constant}, \quad (13)$$

with $b = 6.28$ and $c = 14.4$ as shown in Fig. 7 *b*. Eq. 13 is consistent with a saturation of the ordering effect of cholesterol. Because S is a proper thermodynamic variable, we may combine Eqs. 11 and 13 by standard thermodynamic methods $[dS = (\partial S/\partial T)_x\, dT + (\partial S/\partial x)_T\, dx]$ to obtain:

$$S(x, T) = 1 - a[T - T_1^*(0)] + \frac{bx}{1 + cx}, \quad (14)$$

with

$$T_1^*(x) - T_1^*(0) = \frac{a^{-1}bx}{1 + cx}. \quad (15)$$

Eq. 14 expresses a surprisingly simple universal dependence of S for CSL on x and T with no cross-terms in x and T (except perhaps a small correction at $x = 0.3$). We discuss Eq. 14 further in the next section.

We now consider our results for 16-PC. The temperature dependence of $S_{16\text{-PC}}$ is also found to be fit by the universal form expressed by Eq. 12 as shown in Fig. 6 *b*. We found an identical scaling constant

$$a = [T_0^*(x) - T_1^*(x)]^{-1}$$

to that for CSL within experimental uncertainty. However, for 16-PC, which is more weakly ordered, the

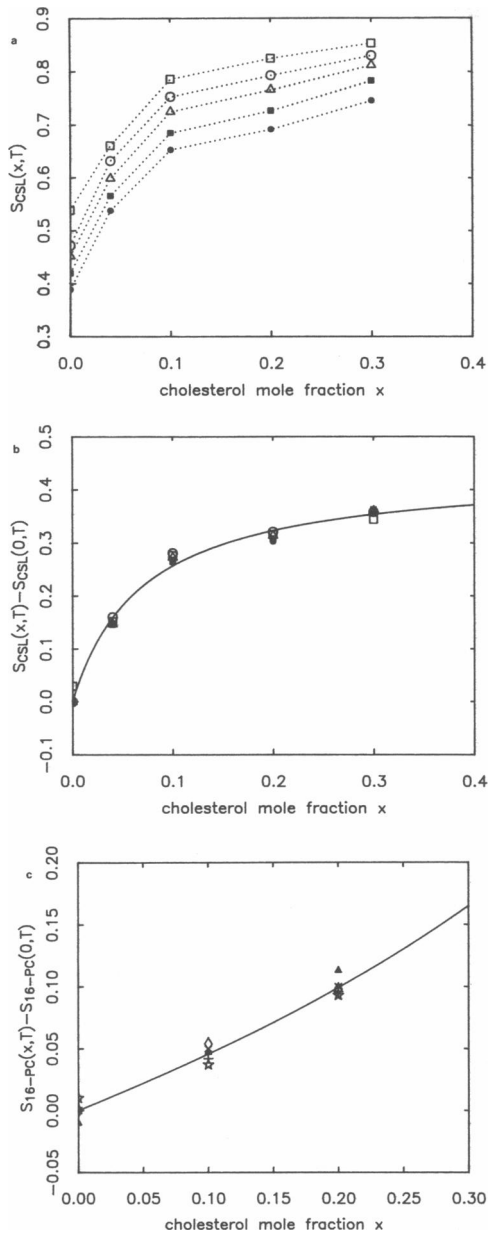

FIGURE 7 (*a*) Plots of $S(x, T)$ for CSL vs. cholesterol mole fraction x. Note the deviation of $S(x, T)$ from linearity in x; 15 (□), 25 (○), 35 (△), 48 (■), and 60°C (●). (*b*) Plots of $S(x, T) - S(0, T)$ vs. x for CSL. A Langmuir isotherm type equation $bx/(1 + cx)$ fits the behavior of $S(x, T) - S(0, T)$ with $b = 6.28$ and $c = 14.4$. (*c*) Same type of plot as *b* for 16-PC for five different temperatures: 15 (+), 25 (×), 35 (◇), 48 (☆), and 60°C (▲). The line is drawn according to Eq. 17a with $d = 0.44$.

reference temperatures $T_1^*(x)$ and $T_0^*(x)$ are different from those for CSL (cf. Table 3). In the case of the x dependence of $S_{16\text{-PC}}$ we obtain results analogous to that of Eq. 13 for S_{CSL} in that $S_{16\text{-PC}}(x, T) - S_{16\text{-PC}}(0, T)$ has a functional form that is (nearly) temperature independent (cf. Fig. 7c), but this functional form is distinctly different from that for CSL, (compare Fig. 7, *c* with *b*).

We now wish to consider a point of view which incorporates the fact that the addition of cholesterol has a similar type of effect on the S_{CSL} and $S_{16\text{-PC}}$ as suggested by their respective temperature dependences, and yet there is a markedly different dependence upon composition. This point of view, simply stated, is that the mixtures of POPC and cholesterol studied here form a simple nonideal solution. Furthermore, because CSL is known to report on cholesterol in model membranes (6, 15), and 16-PC relates to the properties of phosphatidylcholines (27, 29), then we expect that $S_{CSL}(x, T)$ and $S_{chol}(x, T)$ are comparable (or at least the same within a constant multiplicative factor of order unity), and also $S_{16\text{-PC}}(x, T)$ and $S_{POPC}(x, T)$ are comparable (where S_{POPC} as used here would more precisely be related to the ordering at the end of the acyl chain). That is, we may regard CSL as merely a labeled cholesterol molecule and 16-PC as merely a labeled phospholipid molecule in our analysis. Thus the fact that $S_{CSL}(x, T)$ and $S_{16\text{-PC}}(x, T)$ obey the same temperature scaling law, Eq. 12 arises because one has a single simple solution. On the other hand, the different functional dependences of S_{CSL} and $S_{16\text{-PC}}$ upon x could arise from the properties of nonideal solutions.

If the POPC/cholesterol solution were ideal, then we would expect its intensive thermodynamic properties (e.g. partial pressure) to vary linearly with x. Since $S_i(x, T)$ for the ith component is an intensive thermodynamic property such as the partial pressure (37), we expect $S_i(x, T) - S_i(0, T)$ to vary linearly with x in the ideal solution limit (i.e. $x \rightarrow 0$). More specifically, given the tendency of cholesterol to enhance ordering, we would expect that if ideal mixing of lipid and cholesterol were occurring, this enhancement to the ordering of both components would simply be proportional to x. (Such ideal solution type of behavior for $S(x, T)$ has been observed in isomeric mixtures of thermotropic liquid crystals [36]). The very nonlinear dependence of S_{CSL} upon x expressed by Eq. 13 would then imply a nonideal solution (although as $x \rightarrow 0$ we recover the linearity in x expected for an ideal solution). Such nonideality would be the case, if, for example, the cholesterol tends to aggregate and not obey ideal mixing as x increases.

These arguments suggest that the term in Eq. 13, $1/(1 + cx)$, which corresponds to the nonlinear behavior should be related to the activity coefficient γ_{chol} for cholesterol (with the activity $a_{chol} = \gamma_{chol}\, x$). In fact, if we simply set

$$\gamma_{chol} = \frac{1}{1 + cx}, \tag{16}$$

with $c = 14.4$ (corresponding to the solute convention that $\gamma_{chol} \rightarrow 1$ as $x \rightarrow 0$), then the decreasing γ_{chol} with x is

consistent with aggregation of the cholesterol as x increases (38a). Eq. 16 represents the simplest interpretation we can make of the effects of nonideality on S_{CSL}. It leads to the following form for Eq. 13:

$$S(x, T) - S(0, T) = bx\gamma_{chol}. \quad (16a)$$

More generally we might expect higher order terms in γ_{chol} or a_{chol} in Eq. 16a, but a significantly more rapid convergence than just a series expansion in x.

If, indeed, the nonideal dependences of $S_i(x, T)$ upon x are closely related to the respective γ_i, then the $S_i(x, T)$ for the two components of the solution cannot vary independently. More precisely, the activity coefficients of the two components of a solution are interrelated by the Gibbs-Duhem equation (38b):

$$x\, d\, ln\gamma_{chol} = -(1 - x) d\, ln\gamma_{PC}. \quad (17)$$

(We are implicitly assuming that the region within the bilayer consists only of two components, with the third component, water only at the headgroup region and between bilayers [39].)

It is a simple matter to obtain an expression for γ_{PC} from that for γ_{chol} (Eq. 16) by integrating Eq. 17 (utilizing as one set of limits of integration $\gamma_{PC} = \gamma_{chol} = 1$ when $x = 0$). One obtains:

$$\gamma_{PC} = (1 - x)^{-c/(1+c)}(1 + cx)^{-1/(1+c)}. \quad (17a)$$

We now need an expression for $S_{16\text{-}PC}$ analogous to Eq. 16a to compare with the experimental data of Fig. 7 *c*. We find that a form closely analogous to Eq. 16a:

$$S_{16\text{-}PC}(x, T) = S_{16\text{-}PC}(0, T) + dx\gamma_{PC} \quad \text{at constant } T, \quad (17b)$$

with γ_{PC} given in Eq. 17a, leads to good agreement with the data as illustrated in Fig. 7 *c*. In particular, we obtained a temperature-independent $d = 0.44$ within the experimental scatter. It is found from Eq. 16 that γ_{chol} decreases by a factor of five on x increasing from 0 to 0.3, whereas from Eq. 17a γ_{PC} increases only 13% upon x increasing from 0 to 0.2. In other words, our simple analysis shows that the different functional forms of S_{CSL} and $S_{16\text{-}PC}$ vs. x may well be consistent with their differing activity coefficients as required by the Gibbs-Duhem relation for nonideal solutions.

Lateral diffusion vs. order parameters

It is known that in an ideal solution the self diffusion rate should be linear with composition (40). The nonlinear variations of the self-diffusion coefficients observed in this work for POPC/cholesterol solutions are characteristic of a nonideal solution (40–43). It has been suggested that one use the excess self-diffusion coefficient (40, 41) analogous to excess thermodynamic functions, to measure the extent of the deviation from ideality. Simple arguments indicate that such an excess coefficient is negative (positive) for CSL (16-PC) in analogy to cyclohexane/benzene (41) and hexane/nitrobenzene (40) solutions. We shall treat the nonideal characteristics from another perspective.

We now consider whether the lateral diffusion coefficient D of CSL may be related to the ordering S, which we have shown provides a direct measure of solution nonideality. We show in Fig. 8 *a* that at each value of temperature, *ln D* varies linearly with $S^2(x, T)$. More precisely, we empirically find that

$$D(S, T) = D^\circ \exp\{-[\alpha(T)S^2(x, T) + \beta]/RT\}, \quad (18)$$

with $D^\circ = 9.18 \times 10^{-6}\text{cm}^2\text{s}^{-1}$, $\beta = 1303K \cdot R$ and that

$$\alpha(T) = a' + b'/T \quad (18a)$$

with $a' = -3364K \cdot R$ and $b' = 1.303 \times 10^6K^2 \cdot R$ (and R here is the universal gas constant). The validity of Eq. 18 is illustrated in Fig. 8 *b*. The values of $\alpha(T)$ shown in Fig. 8 *c* were obtained from the variation of *ln D* with S for each T, as was the value of $D^\circ(T) = D^\circ e^{-\beta/RT}$. Fig. 8 *b* shows the universal linear curve obtained when $ln[D(x, T)/D^\circ(T)]$ is plotted vs. $\alpha(T)S^2(x, T)/RT$ for each value of x (i.e. constant x behavior).

We have also been able to fit our results on D for 16-PC to an equation of the form of Eq. 18 as illustrated in Fig. 8 *d*. There is somewhat more (random) scatter due in part to the somewhat greater error in our measurements of $D_{16\text{-}PC}$ vs. D_{CSL}. Nevertheless, we find that these results are also well-fit by Eq. 18 with $D^\circ = 1.06 \times 10^{-4}\text{cm}^2\text{s}^{-1}$, $\beta = 2317K \cdot R$ with $a' = -2.60 \times 10^4K \cdot R$ and $b' = 8.56 \times 10^6K^2 \cdot R$. Note that for both probes $\alpha(T)$ decreases monotonically with temperature over the range studied. This smaller value of $\alpha(T)$ at the higher temperatures implies a weaker dependence for D_{CSL} and $D_{16\text{-}PC}$ on S at the higher temperatures. We have tried a variety of different functional forms of *D vs. S*, but only the form of Eq. 18 was successful. This statement must be qualified with the following observation. We were also successful in the case of CSL (but not 16-PC) with fitting our data to a linear dependence of *ln D* vs. $S(x, T)$, and the χ^2 test was comparable to that for Eq. 18 ($\chi^2 \approx 10^{-2}$). We point out in the Discussion section that $\alpha(T)S^2 + \beta$ in Eq. 18 is the activation energy for the lateral diffusion. In the case of the fit of *ln D* vs. $S(x, T)$ for CSL, however, the numerical fit leads to a negative activation energy (and very small D°), which makes no sense physically. We have thus ruled out this latter functional form on physical grounds for CSL and statistical grounds as well for 16-PC.

Rotational diffusion vs. order parameters

We found an interesting universal relation between $R_\perp$ of CSL and its order parameter S in the highly ordered

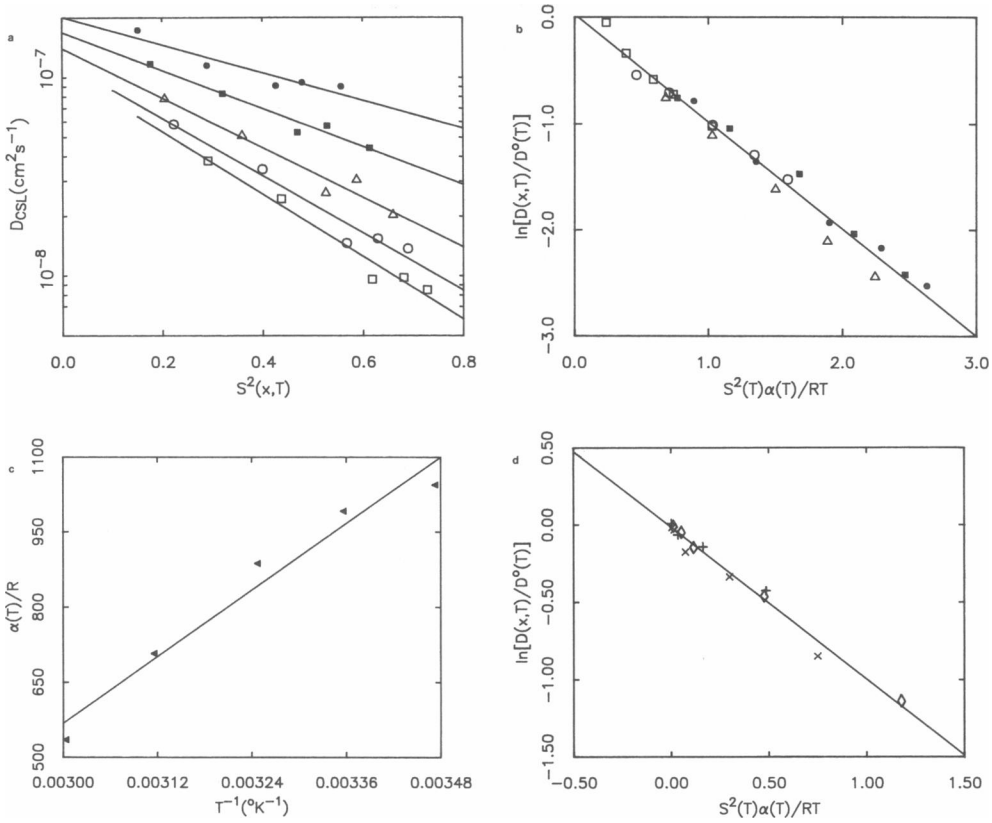

FIGURE 8 (*a*) Semilog plot of D_{CSL} vs. S^2 at different temperatures: 15 (□), 25 (○), 35 (△), 48 (■), and 60°C (●). (*b*) Plots of $[ln(D(x, T)) - ln((D°(T))]$ vs. $\alpha(T)S^2(T)/RT$ for CSL at different compositions: 0 (□), 4 (○), 10 (△), 20 (■), and 30 (●) mol %. (*c*) Plot of $\alpha(T)/R$ vs. T^{-1} associated with *b*. (*d*) Same type of plots as *b* for 16-PC: 0 (+), 10 (×), and 20 mol % (◇).

POPC model membranes containing cholesterol:

$$R_\perp = A(1 - S)^2, \tag{19}$$

with $A = 9.15 \times 10^7\ s^{-1}$. The constant A is independent of both composition and temperature. This universal behavior is illustrated in Fig. 9 for all our data on CSL. On the other hand the form of Eq. 18 or its variants proved unsuccessful.

In the case of $R_\perp$ for 16-PC, we could not find any simple correlation with S (including the forms of Eqs. 18 and 19). In fact, from the data of Table 2 we find that $R_\perp$ increases with S as the latter increases with mole percent cholesterol; on the other hand $R_\perp$ decreases as S is increased by lowering the temperature. Thus, there is no simple relation between $R_\perp$ and S for 16-PC. This is perhaps not surprising, since the motion of the 16-PC nitroxide moiety located at the end of the acyl chain (cf. Fig. 1) is known to depend greatly on the complex internal modes of the chain. The case for the rigid CSL probe is most certainly much simpler.

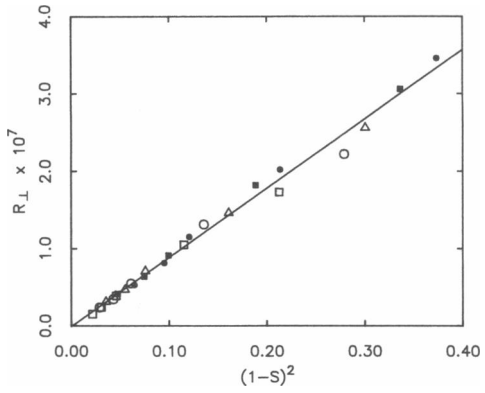

FIGURE 9 Plot showing a universal relation between $R_\perp$ and $(1 - S)^2$ for CSL: 15 (□), 25 (○), 35 (△), 48 (■), and 60°C (●).

Comparison with other work: lateral diffusion

The previous studies of lateral diffusion have almost all focused upon phospholipid diffusion. Our results for D of 16-PC do not exhibit significant influence of cholesterol. The PNSE study of the same system (23), also showed little effect of the cholesterol on the self-diffusion of the POPC molecules, but it showed a small increase compared with our observed small decrease. Only in the FRAP studies of lateral diffusion in DMPC and egg-PC model membranes containing cholesterol (20, 21) were both fluorescence-labeled sterol and phospholipid studied. However, these studies gave significantly different results from ours in three respects. First, the diffusion rates of the fluorescence-labeled sterol and phospholipid probes were nearly the same under all conditions of cholesterol concentration and temperature in the liquid crystalline state. Second, the temperature dependence of self-diffusion coefficient was very mild in all compositions. The activation energies were about 2–3 k cal/mol, which is almost a factor of three less than those of CSL. Third, self-diffusion coefficients of both fluorescence probes were almost constant until the concentration of cholesterol reached 10 mol %, and then they decreased by factors of three at 20 mol %, but they did not change much in the range from 20 to 40 mol %. We believe that the different result from the two experiments, including those with respect to the relative behavior of those two probes, is due to the fact that the photosensitive functional group attached to the parent molecules used in the FRAP experiments is very substantial in size so that it could have a dominant influence on the diffusional process, which could result in identical diffusion coefficients that are different from that of cholesterol and phospholipid.

It was found previously that the major effect of cholesterol is to increase the structural ordering in the bilayer of phosphatidylcholine at low water content (15). In the present work we find that it not only increases the structural ordering but it also reduces the rotational diffusion rate ($R_\perp$) considerably, (although it seems to enhance rotation around molecular long axis, i.e., $R_\parallel$ for CSL). The difference may be due to the low vs. high water content of the bilayer.

DISCUSSION

Our extensive results on order parameter S, rotational diffusion coefficient $R_\perp$, and lateral diffusion coefficient D, and the simple correlations between them both as a function of x (mole fraction of cholesterol) and of T in the liquid crystalline phase (above T_m) are clear and strong manifestations that this is a simple nonideal solution of POPC and cholesterol. This is, of course, in agreement with the observation of Sackmann and co-workers (11) who found a single phase for DMPC/cholesterol mixtures for $x = 0.14$ and possibly as high as 0.45. The order parameter of the CSL molecules which should relate closely to the properties of cholesterol molecules, and of 16-PC, which should relate to the properties of POPC, are simply interpreted in terms of nonideal solutions in the present work. This suggested an approach whereby the activity coefficients are simply given by the deviation of the respective order parameters from linear behavior in x. The diffusion coefficients $R_\perp$ and D also show rather simple and monotonic variation in x and T in this phase. In fact, surprisingly simple correlations with S have been found for them, and hence with the activity coefficients obtained from them. It is perhaps remarkable that such consistent evidence could be obtained from results on these three quite different types of parameters.

In general, we have observed very substantial variations of S, $R_\perp$, and D for CSL as x is increased from zero, whereas only modest changes were observed for 16-PC. While this might naively seem to suggest some peculiarity, we have shown in the previous section that it may simply be due to the Gibbs-Duhem equation applied to γ_{chol} and γ_{POPC}.

The observed γ_{chol} variation with x is consistent with preferential association of cholesterol molecules with each other in the POPC solvent. This leads to values of $\gamma_{chol} < 1$. It is therefore no surprise that D and $R_\perp$ for CSL are modified significantly as x increases from the very dilute limit (i.e. less than 1 mol % of CSL). This tendency to aggregation of the cholesterol (including CSL) molecules means that the environment of CSL changes significantly as a function of x, from that of flexible POPC molecules, to the more rigid cholesterol molecules. One might expect that a cholesterol-rich region would be more dense and compact than the pure POPC bilayer providing less room available for the molecule to diffuse. As a result, the self diffusion of CSL in such a region should be slower than in the pure POPC bilayer. The rotational diffusion will be more restricted by the increased ordering, but this feature has already been included in our rotational model that distinguishes the R-tensor and the restoring potential from which S is calculated (cf. Eq. 8). The cholesterol-rich regions must also be more solidlike due to the dense packing, thereby providing greater frictional resistance to rotational motion, to explain the observed order of magnitude decrease in $R_\perp$ for CSL with x. We do note a substantial increase of activation energy (cf. Table 1) for both D and $R_\perp$.

The tendency of cholesterol to aggregate means that

the POPC-rich regions are less influenced by cholesterol molecules than would otherwise be expected. This is consistent with the rather modest effect of cholesterol on the lateral diffusion of 16-PC. We did observe a small increase in $R_\perp$ for 16-PC with the addition of cholesterol. It might imply that the increase in overall ordering results in a slightly lower friction in the end-chain region (somewhat analogous effects are known in other systems [44]).

Self association, creating larger and more cholesterol-rich regions or clusters, possibly competes with the creation of new clusters in the nonideal solution. The saturation effect on γ_{chol} (hence on S, D, and $R_\perp$) for $cx > 1$ (cf. Eq. 13–16) suggests that in the concentration range ≥ 10 mol % cholesterol, the addition of more cholesterol merely increases the extent, but not the nature of the cholesterol-rich clusters. This may be thought of as a preprecipitation regime of the nonideal solution.

When we consider (*a*) the temperature independence of γ_{chol} and $\gamma_{16\text{-}PC}$, and (*b*) the universal dependence of S for both CSL and 16-PC on the scaled temperature t^U (cf. Eq. 12), these are surprisingly simple results. Related behavior has indeed been seen recently for S_{CSL} in mixtures of nearly identical thermotropic liquid crystals (36), where the temperature was scaled relative to the observed phase-transition temperature at which S_{CSL} was independent of composition.

More unusual perhaps is Eq. 19 expressing $R_\perp$ for CSL simply as proportional to the square of the disorder parameter, $1 - S$. This seems to suggest that for the highly ordered CSL, the rotational dynamics should be referred to the rigid crystalline state of cholesterol, where the disorder parameter would be expected to be zero, and the packing forces imply a near infinite frictional resistance to reorientation. That is, the microviscosity may be expected to be a monotonic function of $(1 - S)^{-1}$. Thus, finding that $R_\perp$ is a function of $(1 - S)$ may not be surprising, although the simplicity of the actual functional form that is found is not, at present, easily explained.

We now wish to consider the S dependence of the lateral diffusion coefficients as expressed by Eq. 18. We can regard $\alpha(T)S^2(x, T) + \beta$ as the activation energy, for the self diffusion as we have already noted. It seems reasonable to interpret this as an enhanced activation barrier to self diffusion as membrane ordering is increased by the addition of cholesterol. In fact, in a theoretical analysis of viscosities in thermotropic liquid crystals (45) an S^2 dependence of the activation energy was predicted in the context of a free volume model. In that theory the relaxation time is proportional to the probability that the molecule finds enough free volume to make translational jumps between two equilibrium positions, and this leads to an S^2 dependent term in the activation energy. There is also, in that theory, a term linear in S in the activation energy which comes from the contribution to the relaxation time arising from the probability that the molecule has enough energy to overcome the potential barrier due to the molecular field created by the other molecules. Diogo and Martins (45) claim that "in most practical cases" the S^2 term is dominant. Our results imply a temperature-dependent activation energy such that the effect of ordering is enhanced at lower T. This could be due to the higher packing (i.e. increased density) as T is reduced, which enhances the role of ordering in providing resistance to diffusion.

All in all, some remarkable empirical relations have been found between $R_\perp$, D, and S in this study of POPC/cholesterol-oriented model membranes by ESR. It should be valuable to further test their universality by similar experiments utilizing different phospholipids in conjunction with cholesterol, as well as phospholipids labeled at other positions along the acyl chain. To gain the full power of ordering and rotational-diffusion studies by ESR, these studies should be performed as a function of orientation of the multilayer in the magnetic field (27), even though such studies would have to be performed after the ESR imaging measurements of lateral diffusion are completed (rather than simultaneously as in the present work).

CONCLUSIONS

(*a*) The ESR-imaging method is a useful and accurate method for measuring lateral diffusion coefficients of nitroxide spin labels in oriented model membranes.

(*b*) POPC/cholesterol mixtures lead to a nonideal solution in the L_α-phase above T_m as evidenced in the measurements of the order parameters, S, the lateral diffusion coefficients, D, and the rotational diffusion coefficients, $R_\perp$, of the spin labels.

(*c*) The nature of the nonideality is consistent with the tendency of the cholesterol molecules to associate.

(*d*) A simple analysis of the order parameters of the spin-labeled components suggests they may be used to estimate activity coefficients of the cholesterol and the phospholipid.

(*e*) Surprisingly simple correlations of (*i*) S vs. x and T, (*ii*) D vs. S, and (*iii*) $R_\perp$ (for CSL) vs. S have been observed in this work which appear to offer insights into the dynamic molecular structure of the model membrane.

APPENDIX

Asymptotic behavior for large ordering potentials and order parameter

The order parameter in Eq. 10 is written in another form,

$$S = \frac{3}{2}\frac{d(ln \int_0^1 \exp[pt^2]\, dt)}{dp} - \frac{1}{2}, \tag{20}$$

where $p = 3/2\,\lambda$. The integral is approximated by

$$\int_0^1 \exp[pt^2]\, dt \sim \frac{e^p}{2p - 3/2}, \tag{21}$$

for reasonably large value of λ. By substituting Eq. 21 into Eq. 20 we have a simple relation between λ and S:

$$\lambda \sim \frac{1}{1 - S} + \frac{1}{2} \quad \text{or} \quad S \sim 1 - \frac{1}{\lambda - 0.5}. \tag{22}$$

The approximate equation (Eq. 22) fits well to the values of the numerical integration when λ is >2.32 ($S > 0.5$) as is seen in Fig. 10. Because the λs are generally >2.5 for CSL in POPC/cholesterol model membranes (except for $x = 0$), we use Eq. 22 to express the temperature dependence of the mean field ordering potential λ. Fig. 6 *a* illustrates the temperature dependence of the order parameter S, which is linear in T, and the slope is independent of the composition. Thus we have from Eq. 11:

$$\lambda \sim \frac{1}{a(T - T_1^*)} + \frac{1}{2} \quad \text{or}$$

$$V(\Omega) \sim -kT\left[\frac{1}{a(T - T_1^*)} + \frac{1}{2}\right] D_{00}^2(\Omega), \tag{23}$$

where T_1^* is a reference temperature at which S becomes 1, and it depends on the composition.

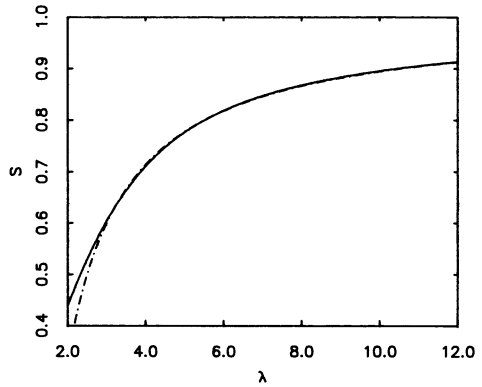

FIGURE 10 Plot of order parameter S vs. ordering potential λ; (—) from numerical integration of Eq. 10 and (—·—) from Eq. 22.

We wish to thank Professor G. Feigenson for his gift of the 16-PC. We thank Dr. D. Cleary and Dr. J. Moscicki for their helpful comments on the ESR-imaging methods used here, and Dr. R. Crepeau and Dr. S. Rananavare for their advice and assistance.

This work was supported by National Institutes of Health grant GM25862 and National Science Foundation grant DMR8604200. Computations were performed at the Cornell National Supercomputer Facility.

Received for publication 6 September 1988 and in final form 16 November 1988.

REFERENCES

1. Gershfeld, N. L. 1978. Equilibrium studies of lecithin-cholesterol interactions. *Biophys. J.* 22:469–488.
2. Mabrey, S., P. L. Mateo, and J. M. Sturtevant. 1978. High sensitivity scanning calorimetric study of mixtures of cholesterol with dimyristroyl- and dipalmitoylphosphatidylcholines. *Biochemistry.* 17:2464–2468.
3. Shimshik, E. J., and H. M. McConnell. 1973. Lateral phase separation in phospholipid membranes. *Biochemistry.* 12:2351–2360.
4. Rubenstein, J. L. R., J. C. Owicki, and H. M. McConnell. 1980. Dynamic properties of binary mixtures of phosphatidylcholines and cholesterol. *Biochemistry.* 19:569–573.
5. Recktenwald, D. J., and H. M. McConnell. 1981. Phase equilibria in binary mixtures of phosphatidylcholine and cholesterol. *Biochemistry.* 20:4505–4510.
6. Presti, F. T., and S. I. Chan. 1982. Cholesterol-phospholipid interaction in membranes. 1. Cholestane spin label studies of phase behavior of cholesterol-phospholipid liposomes. *Biochemistry.* 21:3821–3830.
7. Lentz, B. R., D. A. Barrow, and M. Hoechli. 1980. Cholesterol-phosphatidylcholine interactions in multilamella vesicles. *Biochemistry.* 19:1943–1954.
8. Copeland, B. R. and H. M. McConnell. 1980. The rippled structure in bilayer membranes of phosphatidylcholine and binary mixtures of phosphatidylcholine and cholesterol. *Biochim. Biophys. Acta.* 599:95–109.
9. Hui, S. W., and N.-B. He. 1983. Molecular organization in cholesterol-lecithin bilayers by x-ray and electron diffraction measurements. *Biochemistry.* 22:1159–1164.
10. Levin, I. W., E. Keihn, and W. C. Harris. 1985. A Raman spectroscopic study on the effect of cholesterol on lipid packing in diether phosphatidylcholine bilayer dispersions. *Biochim. Biophys. Acta.* 820:40–47.
11. Knoll, W., G. Schmidt, K. Ibel, and E. Sackmann. 1985. Small-angle neutron scattering study of lateral phase separation in dimyristroylphosphatidylcholine-cholesterol mixed membranes. *Biochemistry.* 24:5240–5246.
12. Hinz, H.-J., and J. M. Sturtevant. 1972. Calorimetric studies of dilute aqueous suspensions of bilayers formed from synthetic L-α-lecithins. *J. Biol. Chem.* 247:3697–3700.
13. Ipson, J. H., G. K. Karlstrom, O. E. Mouritsen, H. Wennerstrom,

and M. J. Zuckermann. 1987. Phase equilibria in the phosphatidylcholine-cholesterol system. *Biochim. Biophys. Acta.* 905:162–172.

14. Godici, P. E., and F. R. Landsberger. 1975. ^{13}C Nuclear magnetic resonance study of the dynamic structure of lecithin-cholesterol membranes and the position of stearic acid spin-labels. *Biochemistry.* 14:3927–3933.
15. Kar, L., E. Ney-Igner, and J. H. Freed. 1985. Electron spin resonance and electron-spin-echo study of oriented multilayers of Lα-phosphatidylcholine water systems. *Biophys. J.* 48:569–593.
16. Kawato, S., K. Kinosita, Jr., and A. Ikegami. 1978. Effect of cholesterol on the molecular motion in the hydrocarbon region of lecithin bilayers studied by nanosecond fluorescence techniques. *Biochemistry.* 23:5026–5031.
17. Smith, L. M., R. M. Weis, and H. M. McConnell. 1981. Measurement of rotational motion in membranes using fluorescence recovery after photobleaching. *Biophys. J.* 36:73–91.
18. Wu, E.-S., K. Jacobson, and D. Papahadjopoulos. 1977. Lateral diffusion in phospholipid multilayers measured by fluorescence recovery after photobleaching. *Biochemistry.* 16:3936–3941.
19. Rubenstein, J. L. R., B. A. Smith, and H. M. McConnell. 1979. Lateral diffusion in binary mixtures of cholesterol and phosphatidylcholines. *Proc. Natl. Acad. Sci. USA.* 76:15–18.
20. Alecio, M. R., D. E. Golan, W. R. Veatch, and R. R. Rnado. 1982. Use of a fluorescent cholesterol derivative to measure lateral mobility of cholesterol in membranes. *Proc. Natl. Acad. Sci. USA.* 79:5171–5174.
21. Golan, D. E., M. R. Alecio, W. R. Veatch, and R. R. Rando. 1984. Lateral mobility of phospholipid and cholesterol in the human erythrocyte membrane: effect of protein-lipid interactions. *Biochemistry.* 23:332–339.
22. Kuo, A.-L. and C. G. Wade. 1979. Lipid lateral diffusion by pulsed nuclear magnetic resonance. *Biochemistry.* 18:2300–2308.
23. Lindblom, G., L. B. A. Johansson, and G. Arvidson. 1981. Effect of cholesterol in membranes. Pulsed nuclear magnetic resonance measurements of lipid lateral diffusion. *Biochemistry.* 20:2204–2207.
24. Fahey, P. F., D. E. Koppel, L. S. Barker, D. E. Wolf, E. L. Elson, and W. W. Webb. 1976. Lateral diffusion in planar lipid bilayers. *Nature (Lond.).* 195:305–306.
25. Hornak, J. P., J. K. Moscicki, D. J. Schneider, and J. H. Freed. 1986. Diffusion coefficients in anisotropic fluids by ESR imaging of concentration profiles. *J. Chem. Phys.* 84:3387–3395.
26. Cleary, D., Y.-K. Shin, D. J. Schneider, and J. H. Freed. 1988. Rapid determination of translational diffusion coefficients using ESR-imaging. *J. Magn. Res.* 79:474–492.
27. Tanaka, H., and J. H. Freed. 1984. Electron spin resonance studies on ordering and rotational diffusion in oriented phosphatidylcholine multilayers: evidence for a new chain ordering transition. *J. Phys. Chem.* 88:6633–6644.
28. Crepeau, R., S. Rananavare, and J. H. Freed. 1987. Automated least squares fitting of slow-motional ESR spectra. Abstracts of the 10th International EPR Symposium. Rocky Mountain Conference. Denver, CO.
29. Birrell, G. B., and O. H. Griffith. 1976. Angle of tilt and domain structure in dipalmitoylphosphatidylcholine multilayers. *Arch. Biochem. Biophys.* 172:455–462.
30. Hubbell, W. L., and H. M. McConnell. 1971. Molecular motion in spin-labeled phospholipids and membranes. *J. Am. Chem. Soc.* 93:314–320.
31. Jost, P. C., and O. H. Griffith. 1973. The molecular reorganization of lipid bilayers by osmium tetraoxide. A spin-label study of orientation and restricted *y*-axis anisotropic motion in model membrane system. *Arch. Biochem. Biophys.* 159:70–81.
32. Freed, J. H. 1976. The theory of slow tumbling ESR spectra for nitroxides. *In* Spin Labeling, Theory and Applications. L. J. Berliner, editor. Academic Press, Inc., New York. 53–132.
33. Meirovitch, E., D. Igner, E. Igner, G. Moro, and J. H. Freed. 1982. Electron spin relaxation and ordering in smectic and supercooled nematic liquid crystals. *J. Chem. Phys.* 77:3915–3938.
34. Schneider, D. J., and J. H. Freed. 1989. Calculating slow motional magnetic resonance spectra: a user's guide. *In* Spin Labeling, Theory and Application, III. L. J. Berliner, editor. Plenum Publishing Corp., New York. In press.
35. Meirovitch, E., and J. H. Freed. 1984. Molecular configuration, intermolecular interactions and dynamics in smectic liquid crystals from slow motional ESR lineshapes. *J. Phys. Chem.* 88:4995–5004.
36. Rananavare, S. B., V. G. K. M. Pisipati, and J. H. Freed. 1987. Nematic ordering near a tricritical nematic-smectic A phase transition. *Chem. Phys. Lett.* 140:255–262.
37. de Gennes, P. G. 1974. The Physics of Liquid Crystals. Oxford University Press, London. 23.

38a. Lewis, G. N., and M. Randall. 1961. Thermodynamics. McGraw-Hill Book Co., New York. 283–284.

38b. Lewis, G. N., and M. Randall. 1961. Thermodynamics. McGraw-Hill Book Co., New York. 261.

39. Houslay, M. D. 1982. Dynamics of Model Membranes. John Wiley & Sons Ltd., Chichester, UK. 51–81.
40. Hawlicka, E., and W. Reimschuessel. 1981. Component self-diffusion in liquid binary solutions. *Ber. Bunsen-ges. Phys. Chem.* 85:210–214.
41. Reimschuessel, W., and E. Hawlicka. 1977. Self-diffusion in benzene-cyclohexane solutions. *Ber. Bunsen-ges. Phys. Chem.* 81:1221–1224.
42. Hawlicka, E., and W. Reimschuessel. 1980. Self-diffusion of components in aniline-benzene solution. *Ber. Bunsen-ges. Phys. Chem.* 84:1119–1121.
43. Anderson, J. E., and W. E. Gerritz. 1970. Molecular motion and spatial order in liquids: the aniline/cyclohexane system. *J. Chem. Phys.* 53:2584–2589.
44. Hwang, J. S., K. V. S. Rao, and J. H. Freed. 1976. An electron spin resonance study of the pressure dependence of ordering and spin relaxation in a liquid crystalline solvent. *J. Phys. Chem.* 80:1490–1501.
45. Diogo, A. C., and A. F. Martins. 1982. Order parameter and temperature dependence of the dynamic viscosity of nematic liquid crystals. *J. Physique.* 43:779–786.